Feasibility of a Stack Integrated SOFC Optical Chemical Sensor

Final Report

Reporting Period Start Date: 10/1/2004
Reporting Period End Date: 9/30/2007

Principal Author: Dr. Michael A. Carpenter

Date Report Issued: 12/21/2007

DOE Award Number: DE-FG26-04NT42184

College of Nanoscale Science and Engineering
University at Albany-SUNY
Albany, NY 12203
Phone: 518-437-8667
Fax: 518-437-8603
Email: mcarpenter@uamail.albany.edu

Disclaimer

Abstract

The DOE-NETL Innovative Concepts (IC) phase II program investigated the feasibility of harsh environment compatible chemical sensors based on monitoring the surface plasmon resonance (SPR) bands of metal nanoparticle doped YSZ nano-cermets, as a function of fuel concentrations, impurities e.g. CO and temperature(500-900°C). In particular, Au nanoparticles (AuNPs) exhibit a strong surface plasmon resonance (SPR) band whose shape and spectral position is not only highly dependent on the refractive index of the host medium but also on chemical reactions at the interface between the metal and the surrounding environment.

Studies have been completed on the oxygen and temperature dependence of the SPR band of the AuNPs, CO sensing studies, oxygen/hydrogen titration experiments, ethanol sensing studies and finally NO_2 sensing studies. Reversible changes in the SPR band are observed for all chemical exposure studies with the sensing mechanism being determined by the oxidative or reductive properties of the exposure gases. Reactions which remove charge from the AuNPs was observed to cause a redshift in the SPR band, while charge donation to the AuNPs causes a blue shift in the SPR band. CO, hydrogen and ethanol in air mixtures were all reductive in nature as they reacted with the YSZ bound oxygen anions forming CO_2 or H_2O thus ultimately inducing charge donation to the AuNPs and a blue shift in the SPR band. While NO_2 and oxygen were oxidative and induced the production of YSZ bound oxygen anions, charge removal from the AuNPs and a redshift in the SPR band.

Table of Contents

Executive Summary

Studies have been completed on the oxygen and temperature dependence of the SPR band of the AuNPs, CO sensing studies, oxygen/hydrogen titration experiments, ethanol sensing studies and finally NO_2 sensing studies. Reversible changes in the SPR band are observed for all chemical exposure studies with the sensing mechanism being determined by the oxidative or reductive properties of the exposure gases. Reactions which remove charge from the AuNPs was observed to cause a redshift in the SPR band, while charge donation to the AuNPs causes a blue shift in the SPR band. CO, hydrogen and ethanol in air mixtures were all reductive in nature as they reacted with the YSZ bound oxygen anions forming CO_2 or H_2O thus ultimately inducing charge donation to the AuNPs and a blue shift in the SPR band. While NO_2 and oxygen were oxidative and induced the production of YSZ bound oxygen anions, charge removal from the AuNPs and a redshift in the SPR band. Details of the studies performed during this program are summarized below.

We have performed a series of experiments to determine the proof of concept for using Au-YSZ nanocomposite films for the detection of CO, NO_2, H_2 and ethanol under harsh environment conditions. These experiments have shown that the sensing mechanism for detection of the reducing gases, CO, H_2 and ethanol, that there is a reaction between the target gas with the O^{2-} ions which occupy vacancies in the YSZ matrix, thus forming an oxidized product with the electrons from the oxygen anion being donated back to the AuNPs nanoparticles which induces the characteristic blue shift of the SPR band. The temperature and oxygen titration experiments confirm that for this reaction to take place, the operation temperature must be above the threshold required for formation of O^{2-} from the background oxygen and if there is no background oxygen or the temperature is below this formation threshold, the reaction is deactivated and sensing is not possible. For the studies performed here the operation temperature needs to be above 400 °C with 500 °C being preferable. Likewise the oxygen titration experiments determined that for CO and H_2 as long as the oxygen levels are above ~8% the reactions are independent of the oxygen concentration. Experiments to determine the oxygen and temperature dependences of the hydrocarbon reactions will need to be done in a future phase of this program. The NO_2 reaction proceeds through the catalytic reduction of NO_2 on hot gold surfaces to form NO and an O atom. The resulting oxygen atom then forms an O^{2-} ion thus removing electrons from the gold nanoparticle causing the characteristic redshift of the SPR band. For this reaction background oxygen actually reduces the signal contrast. Thus by reducing oxygen levels to 5 and 10vol.% the sensing signal for NO_2 increases as there are more sites available for the formation of a O^{2-} ion as the sample is not saturated from the background oxygen concentration. Therefore the detection of NO_2 is dependent on the background oxygen levels even between 5 and 20vol.% oxygen and is also dependent on temperature as it does have to be above the threshold for O^{2-} formation.

The detection limits for NO_2 were determined to be 5ppm in an air carrier gas and at 500°C. The detection limits for CO were not pushed strongly but at 1000ppm still showed strong signal changes implying that 100ppm detection limits with these initial films is likely possible. For the H_2 studies we were able to detect concentrations as low as 500ppm with strong signal to noise ratios implying a detection limit of ~250ppm. Since the ethanol studies have only been preliminary detection limits cannot be estimated however the significant result from these studies is that they did not appear to become poisoned with carbon within the 20hrs of run time thus

performed. Furthermore, all of the films used for this study have shown to be quite rugged and within the lifetime of this study have not shown any significant degradation with time or chemical exposure. Therefore in conclusion it appears that the all-optical detection of CO, H_2, NO_2 and hydrocarbons using the optical signature of Au nanoparticles embedded in a YSZ matrix has shown strong promise for use as a harsh environment compatible chemical sensor.

A detailed electrochemical model was developed and tested for the O_2/H_2 and O_2/NO_2 titration experiments and since the peak position of the SPR band relies closely on the number of driven oscillating free electrons per gold nanoparticle, we were able to monitor electrochemical charge transfer from Au nanoparticles to diffusing oxygen ions by monitoring the optical properties of the Au-YSZ nanocomposite thin film. A direct relation was observed for the change in the equilibrium ratio, $pH_2^{1/4}/pO_2^{1/8}$ for the O_2/H_2 system and $pO_2^{-1/8}\,pNO_2^{-1/4}$ for the O_2/NO_2 system, contributing to the oxidation and reduction of the YSZ and the change in the square of the SPR band peak position. Free electron theory states that this change in the square of the SPR band peak position is directly proportional to the change in conduction electrons available per Au nanoparticle, thus our observations agree with the expected trend for charge transfer versus the redox gas mixture.

Experimental Methods:

Au-YSZ thin films have been deposited using rf co-magnetron confocal physical vapor deposition (PVD) from a Au target (99.99% purity) and a 5 wt % Y_2O_3-ZrO_2 target (99.9% purity), purchased from Williams Advance Materials (Brewster, NY). Shutters obstructing the substrates from the targets were opened after 15 minutes of stabilization at deposition power and the films were deposited in 5 minutes on sapphire substrates in a 5 mTorr Ar environment. Depositions took place with the Au target at 20 W and the YSZ target at 200 W to ensure a ~10 at. % Au composition in the nanocomposite film.[1,2] After deposition, films were removed from the deposition chamber and placed into an annealing chamber. The films were then annealed at ~900 °C for 2 hours under ~1800 sccm of Ar at atmospheric pressure. Figure 1 is XRD data acquired for a typical post annealed Au-YSZ film on a sapphire substrate, which provides an approximate average grain size for both the Au and the YSZ at ~28 nm using the Scherrer formula. Film thicknesses of the deposited films were ~30nm as measured using scanning electron microscopy.

After annealing and characterization, the Au-YSZ films are placed in a Macor sample holder centered in an optically transparent quartz flow cell housed in a tube furnace. Collimated light is transmitted through the film and is analyzed using an Oriel Instruments (Stratford, CT) MS257 monochromator equipped with a Peltier cooled CCD. As schematically depicted in Figure 2, the gas exposure bench schematic shows an expanded view of the Au-YSZ film deposited on the sapphire substrate. This expanded view shows only half of the 1 cm diameter sapphire substrate is coated with a Au-YSZ film. This film coverage is achieved through the use of a shadow mask during the PVD process and allows for online background data correction to be performed on every spectrum acquired by the monochromator, resulting in more accurate absorption data acquired for the Au-YSZ thin films. The total gas flow was held at 2000 sccm with gas mixtures controlled by MKS (Wilmington, MA) mass flow controllers attached to a stainless steel gas flow manifold coupled to the quartz flow cell inlet.

<u>Oxygen Titration Experiments</u>

From our initial experiments with CO reacting with the Au-YSZ nanocomposites during Year 1 it was clear that the reaction had a dependence on the oxygen content. Therefore our mechanism studies have begun with a series of oxygen titration experiments. Exposure studies using a CO in N_2 gas mixture showed no change in the SPR band, while those using CO in air mixtures showed a reversible change in the SPR band. Furthermore, by simply switching from a N_2 gas to an air gas at an operating temperature of 500°C there was a slight redshift and more notable broadening of the SPR band as shown in Figure 3. It is well established in the literature that the YSZ matrix is an oxygen ion conductor at elevated temperatures, and above a given thermal threshold O_2 dissociates on YSZ and generates O^{2-} ions which occupy the vacancies within the crystalline lattice of YSZ. To confirm our suspicions that the change in the SPR band observed in Figure 3 was due to the generation of O^{2-} ions we performed a study of the temperature dependence of the SPR band in both air and N_2 environments. The graph in Figure 4 displays a consistent broadening of the SPR band between room temperature and 600°C for both carrier gases. This is consistent with the increase in the scattering of the surface plasmons. However, for the air mixture at ~350°C there is a considerable increase in the FWHM and above this temperature the rate of change in the FWHM is the same as the lower temperature data. This sudden jump in the FWHM occurs at a temperature which is consistent with the onset of O^{2-}

formation on the YSZ matrix. Since the SPR band also has an oxygen dependence we have performed a series of oxygen titration experiments which mixed 99.999% pure N_2 mixed with 99.999% pure O_2 for oxygen concentrations ranging from 0.1% to 10%, with a standard air mixture serving as the data point for 20% O_2 in N_2. The peak position and the FWHM of the SPR band as a function of O_2 at an operating temperature of 500°C are displayed in Figure 5a and b respectively. The peak position slightly red shifts at low concentrations and saturates at concentrations above 2.5%, while the FWHM continuously broadens and nearly saturates between the 10 and 20% values. Since we can assume that O^{2-} ions are formed at this operating temperature, it is apparent that the increase in O^{2-} concentration causes these characteristic changes in the SPR band through the charge removal and subsequent positive charge buildup on the Au nanoparticles. The fundamental mechanism and theoretical understanding of these changes on the optical properties of the Au nanoparticles was studied in more detail during the H_2/O_2 titration experiment described in detail later in this report.

CO Sensing Studies

The sensing studies started with CO exposure experiments in the sensor test station described earlier. These studies used 30nm thick Au(10at%)-YSZ films which were annealed to 900°C, resulting in YSZ and Au grain sizes of ~19nm as determined by X-ray diffraction studies.[1] Sequential exposures to air and CO/air gas pulses at 500°C resulted in a slight blue shift and a significant narrowing of the SPR band as seen in Figure 6. The data were fitted with Lorentzian curves and the insetted graph of Figure 6 displays the difference spectra determined from subtracting the gas on and gas off absorption data. The CO sensing signal is taken as the intensity value determined from points A & B in the insetted graph and a series of CO exposures are displayed in Figure 7. As can be seen the optical properties reversibly change upon exposure to sequential air and air/CO exposures at an operating temperature of 500°C. The response time of the CO sensing signal is ~40s and the recovery time displays a 2-stage process with a fast, ~60s, and slow, ~1000s, recovery time. The sensing mechanism has been attributed to high temperature interfacial charge transfer chemical reactions, occurring at the perimeter of the Au nanoparticles, which inject charge into the Au nanoparticle, causing changes in both the position and shape of the SPR band. These reactions are presumed to be associated with the reduction of the YSZ matrix and the oxidation of CO, via a charge transfer reaction between YSZ bound oxygen anions, formed through the dissociative adsorption of oxygen molecules on YSZ at high temperatures, and the Au nanoparticles. We have performed CO exposure studies in the absence of oxygen at 500°C and observed no change in the SPR band, while CO exposures as a function of temperature likewise did not produce a change in the SPR band until temperatures exceeded ~350°C, which is the same temperature required for O^{2-} formation and transport within YSZ materials. We have also studied the temperature dependence of the CO reaction and its corresponding change in the Au nanoparticle SPR band. Exposure studies from room temperature to 500°C have been performed for 1% CO mixtures in air as shown in Figure 8. As can be seen the 1% CO exposures have no affect on the SPR band for temperatures below 325°C and then suddenly turn on at 400 and 500°C. Again this onset in the reaction is consistent with the O^{2-} formation temperature on the YSZ matrix. The CO sensing studies and results are discussed in more detail in our publication from 2006.

Hydrogen/Oxygen Titration and Sensing Studies

As a continuation of our studies we performed a series of experiments to demonstrate the detection of hydrogen under harsh conditions as this is relevant for potential SOFC applications, and furthermore the H_2/O_2 titration experiment allowed for the testing and development of a detailed theoretical model for the proposed charge transfer sensing mechanism first outlined in the oxygen titration experiments and also in the CO sensing studies. Four exposure experiments were performed each running a total of ~48 hours long, followed by a temperature reduction from 500 °C to room temperature between each individual exposure experiment. During the duration of the experiments the H_2 concentration was alternately varied from zero to 0.05, 0.1, 0.2, 0.5 and 1.0 vol. % in a constant concentration of O_2 and N_2. These cycles of low to high H_2 concentration were repeated in 0.1, 0.2, 0.5, 1.0, 2.5, 5.0, 7.5, and 10 vol. % concentrations of O_2. Each individual gas mixture was held constant for 31 minutes where ten SPR band spectra were acquired and averaged every 10 seconds for the first minute of a new gas exposure and every minute for the remaining 30 minutes of the gas exposure concentration. Upon completion of the exposure experiment the oven was turned off and the Au-YSZ film was cooled to room temperature under a 1000 sccm flow of N_2. Once ambient conditions were reached the flow cell was evacuated to 5 torr where it remained until the next exposure experiment.

Since YSZ is optically transparent, the optical data acquired by the monochromator is indicative of the optical absorption of the Au nanoparticles (AuNPs) embedded in the YSZ films. The optical absorption due to AuNPs can be separated into two parts based on the electronic structure of the nanoparticles: (1) photon absorption by interband electrons and (2) photon absorption by the quasi-free electrons in the metal nanoparticle; this research relies on monitoring the latter. The forced oscillation of quasi-free electrons by absorption of electromagnetic radiation results in a SPR resonance band, which can be approximated as a Lorentzian for metal nanoparticles[1]. There is expected to be some overlap in both the interband and the quasi-free electron photon absorption for AuNPs, but by embedding the AuNPs in a high dielectric constant material such as YSZ (ε_m=4.41)[2] one is able to "decouple" the absorption due to the two electron states. This tactic does not entirely deconvolute the SPR band from the interband transition absorption, so Lorentzians are only fit to the SPR bands between photon wavelengths 550 and 850 nm, which limits the convolution of the high energy photon absorption by interband electrons. Examples of these fits are displayed in Figure 9 for the Au-YSZ film exposed to various H_2/O_2 gas exposure conditions. The fitted full width at half maximum (FWHM) and peak position values from data such as these are then used to monitor the redox state of the YSZ matrix.

Theoretical Calculations:

When examining the optical properties of metal nanoparticles, there are simple models used to describe the resonance of the quasi-free electrons of small nanoparticles ($R_{NP} << \lambda$) exposed to electromagnetic radiation. As mentioned earlier, this SPR resonance is typically modeled as a Lorentzian curve where the bandwidth of the SPR band is indicative of the excitation lifetime of quasi-free electrons at resonance and the peak position is related to the particle charge density. The primary focus of this titration study was to examine the electrochemical charge transfer between AuNPs and oxygen ions in the YSZ matrix and for this reason the SPR bandwidth will not be discussed at this time. By application of electrostatics the SPR band peak position (ω_1) of small spherical nanoparticles ($R_{NP} << \lambda$) can be described by equation 1:

$$\omega_1 = \sqrt{\frac{3Ne^2}{(1+2\varepsilon_m)m_e 4\pi\varepsilon_0 R^3}}\,, \tag{1}$$

where N denotes the number of conduction electrons per particle, e is the elementary charge, ε_m is the dielectric function of the matrix, m_e is the electron mass, ε_0 is the permittivity of free space, and R is the particle radius.

With the above relation, charge transfer can be described by monitoring the peak position of the SPR band. However, there is still the matter of discerning how the electrochemical reaction occurring within the Au-YSZ thin film results in the charging and discharging of the AuNPs.

As mentioned previously, exposure to varying concentrations of H_2 and O_2 in N_2 at 500 °C has been performed to reduce and also to oxidize the YSZ matrix, so it is crucial to understand how charge is expected to transfer to and from the AuNP upon various exposure conditions. For this, a half reaction can be written in Kröger-Vink notation for the reduction of the YSZ matrix by gas phase H_2:

$$\mathrm{H_{2(g)} + O_O^{\times} + 2Y'_{Zr} \longleftrightarrow H_2O_{(g)} + V_O^{\bullet\bullet} + 2Y'_{Zr} + 2e'_{AuNP}}\,, \tag{2}$$

and another half reaction can be written for the oxidation of the YSZ matrix by gas phase O_2:

$$\mathrm{O_O^{\times} + 2Y'_{Zr} \longleftrightarrow \frac{1}{2}O_{2(g)} + V_O^{\bullet\bullet} + 2Y'_{Zr} + 2e'_{AuNP}}\,. \tag{3}$$

It is important to note that the notation used for a neutrally charged oxygen atom in an oxygen lattice site: $\mathrm{O_O^{\times}}$, is also what will be referred to as an oxygen ion which has diffused into or out of the YSZ matrix, oxidizing or reducing the matrix, respectively. It is charge neutral in Kröger-Vink notation due to the charge screening by the double charged oxygen vacancies. By combining the two previous half reactions we can derive a reaction equation that accounts for all charge transfer at varying concentrations of H_2 and O_2:

$$\mathrm{H_{2(g)} + 2O_O^{\times} + 4Y'_{Zr} \longleftrightarrow H_2O_{(g)} + \frac{1}{2}O_{2(g)} + 2V_O^{\bullet\bullet} + 4Y'_{Zr} + 4e'_{AuNP}}\,. \tag{4}$$

When at equilibrium the full reaction can be written in terms of the equilibrium constant K:

$$K = \frac{p\mathrm{H_2O}\,p\mathrm{O_2}^{1/2} N_{V_O^{\bullet\bullet}}^2 N_e^4}{p\mathrm{H_2} N_{O_O^{\times}}^2}\,, \tag{5}$$

where $p\mathrm{H_2}$, $p\mathrm{H_2O}$, and $p\mathrm{O_2}$ represent the numeric value of the partial pressures of H_2, H_2O and O_2, respectively and $N_{O_O^{\times}}$, $N_{V_O^{\bullet\bullet}}$ and N_e correspond to the number of filled oxygen vacancies, unfilled oxygen vacancies and AuNP conduction electrons per film volume containing one AuNP and the corresponding YSZ per AuNP. For this model we assume that the total positive charge of the AuNP is equal to two times the number of filled oxygen vacancies ($N_{O_O^{\times}}$) and that the number of unfilled vacancies ($N_{V_O^{\bullet\bullet}}$) is equal to the total number of vacancies available when the AuNP is uncharged ($N_{V_O^{\bullet\bullet}0}$) minus the total number of filled oxygen vacancies ($N_{O_O^{\times}}$). With these assumptions, (5) can be reformulated as the following:

$$\frac{K^{1/2} p\mathrm{H_2}^{1/2}}{p\mathrm{H_2O}^{1/2}\, p\mathrm{O_2}^{1/4} N_e^2} = \frac{2N_{V_O^{\bullet\bullet}0}}{N_{e0} - N_e} - 1\,, \tag{6}$$

where N_{e0} denotes the number of conduction electrons in an uncharged AuNP. Simplifications can be made to (6) if it is assumed that the number of unfilled oxygen vacancies is always greater than the number of filled oxygen vacancies results in the following quadratic equation:

$$\frac{2N_{V_O^{\cdot\cdot}0}\,pH_2O^{1/2}\,pO_2^{1/4}}{K^{1/2}\,pH_2^{1/2}}N_e^2 + N_e - N_{e0} \cong 0\,. \tag{7}$$

By solving the quadratic equation and making simplifications based on the magnitude of $N_{V_O^{\cdot\cdot}0}$ and N_{e0}, the relation that correlates the number of conduction electrons per AuNP to the exposure gas partial pressures, $N_{V_O^{\cdot\cdot}0}$, N_{e0}, and the equilibrium constant is the following:

$$N_e \cong \sqrt{2}\left(\frac{K^{1/2}N_{e0}}{N_{V_O^{\cdot\cdot}0}\,pH_2O^{1/2}}\right)^{1/2}\frac{pH_2^{1/4}}{pO_2^{1/8}}\,. \tag{8}$$

By solving (1) for N_e and combining this with (8), one is left with an equation where the square of the SPR band peak position should vary linearly with $pH_2^{1/4}/pO_2^{1/8}$:

$$(\omega_1)^2 = \sqrt{2}\left(\frac{3e^2}{(1+2\varepsilon_m)m_e 4\pi\varepsilon_0 R^3}\right)\left(\frac{K^{1/2}N_{e0}}{N_{V_O^{\cdot\cdot}0}\,pH_2O^{1/2}}\right)^{1/2}\frac{pH_2^{1/4}}{pO_2^{1/8}} \tag{9}$$

Results and Discussion:

Changes in the absorption spectrum of Au-YSZ thin films towards changes in redox environment has already been demonstrated for varying concentrations of CO in air,[Error! Bookmark not defined.] and a simple mechanism has been proposed which accounts for the changes observed in the SPR band upon exposure to CO. In summary as CO reacts with a filled oxygen vacancy it forms CO_2 and electrons are donated back to the AuNP causing a blue shift in the SPR band.[Error! Bookmark not defined.] Though this proposed mechanism agrees qualitatively to the changes in the SPR band, further analysis of a slightly different reaction has been performed for this H_2/O_2 titration study in order to quantitatively justify the proposed mechanism. The mechanism relies on electrochemical reactions between the exposure gases, the catalytic AuNPs and the YSZ matrix, and for the current work these reactions have been outlined in the previous section for exposure to O_2 and H_2. It is also expected that exposure to varying concentrations of H_2O would also have an affect on the SPR band of the AuNPs embedded in the YSZ matrix. The gases used for these experiments were all of high purity and while H_2O concentrations were not varied or monitored for the experiments performed for this work, the background H_2O concentration is assumed to be minor and of a constant value for the purposes of this calculation. In addition, experiment to experiment variations in the baseline (initial experimental exposure) peak position of the SPR band of AuNPs at 500 °C and under a flow of 0.1 vol. % O_2 in N_2 were also observed. These peak shifts may be caused by slight variations in the thermal calibration parameters or by ambient climate changes. These baseline changes had no major affect on the observed electrochemical reactions and will be discussed in further detail later in this manuscript.

After absorption data was collected for a full 48+ hour exposure experiment, Lorentzian fits were performed like the ones outlined in Figure 9 to determine the peak position (ω_1, λ_1) and full width at half maximum (FWHM) as a function of time. Figure 10-A displays a typical peak position vs. time plot while Figure 10-B displays the FWHM vs. time data set for a Au-YSZ thin film. As mentioned previously, the entire experiment was repeated 4 times and each repeated experiment resulted in a similar set of data, where exposure to greater concentrations of H_2 resulted in a blue shift and narrowing of the SPR band, and increasing concentrations of O_2 resulted in a red shift and broadening of the SPR band. Since one possible application for Au-YSZ thin films is in harsh environment gas sensing, it is important to also note that Figure 10 displays stable responses to changes in gas exposure concentrations over an almost two day time

period and was repeatable over the 4 experimental trial. While extensive reliability tests will be required these initial tests demonstrated that long exposure stability is a promising characteristic for potential future sensor applications including aerospace or within the solid oxide fuel cell industry where gas sensors are required to withstand long term exposures to harsh environments.

As mentioned previously, the primary concern of this communication is to establish an understanding of the electrochemical charge transfer characteristics between embedded AuNPs and oxygen ions within the YSZ matrix and it is this reason that an in depth analysis of the FWHM data will not developed for this paper. However, as seen in Figure 10-B the FWHM is monitored as a function of time and it is understood that this broadening and narrowing of the SPR band is due to increases and reductions, respectively, in quasi-free electron relaxation times.[19] An in-depth study is currently underway to examine the changes seen in the FWHM of the SPR band as the gas exposure environment is varied. However, as one would expect, there are several factors that can affect the SPR band FWHM, including electron density, dielectric function of the matrix, and defects surrounding the AuNPs. Of primary interest to this research is an effect called adsorbate induced dampening, which has been primarily studied for metal nanoparticles experiencing cryogenic gas adsorption.[3,4] Future studies of this system will be aimed at research determining the energy shifts in electron defect states in the YSZ matrix upon oxidation and reduction. This information is critical so that a clear model for adsorbate induced dampening of the SPR band at elevated temperatures for nanoparticles embedded in metal oxides can be developed and compared to what is observed experimentally.

After fits are performed for the SPR band absorption data as a function of time, the peak position at equilibrium can be averaged for the various gas concentrations. Figure 11 displays the peak position for various concentrations of H_2 as a function of O_2 concentration for the data seen in Figure 10-A. A dashed line connecting the data points for each H_2 concentration has been added to guide the eye along each data set, all of which exhibit a negative power dependence, which is expected from equation (9). A random SPR band peak position baseline shift is experienced from experiment to experiment, as mentioned previously, so averaging the peak position data from experiment to experiment results in a rather large standard deviation compared to the relative scale from data point to data point, even though the data follows the same gas concentration dependence for every experiment. For this reason, the change in peak position of the SPR band in relation to the peak position in the absence of hydrogen, for the four H_2/O_2 gas titration experiments were averaged and are displayed in Figure 12.

Qualitatively, Figure 12 suggests that with O_2 in excess, a given concentration of H_2 will always result in the same blue shift of the SPR band, which implies that the same number of electrons are donated back into the AuNP for that H_2 exposure, irregardless of the O_2 concentration. Specifically at O_2 concentrations above 5%, all of the H_2 gas exposures have a constant blue shift in the SPR band, while at the lowest H_2 concentrations, 0.2, 0.1 and 0.05%, oxygen concentrations of 1% and above induce a constant blue shift in the SPR band. Furthermore, Figure 12 also suggests that at low O_2 concentrations, Au-YSZ thin films are more sensitive to changes in H_2.

It is assumed that oxidation and reduction of the YSZ matrix by the O_2 and H_2 concentrations used in this study, respectively, results only in oxygen ion diffusion into and out of the vacancies

paired by two yttrium ions as shown in reaction (4). With this assumption, what is expected is a linear relation between the square of the peak position and the ratio: $pH_2^{1/4}/pO_2^{1/8}$, as indicated in equation (9), which is plotted in Figure 13 for all four collected data sets. Plotted on the secondary ordinate is the calculated number of conduction electrons per nanoparticle based on the peak position using the electrostatic relation between peak position and number of conduction electrons (1). As mentioned previously, there appears to be a random baseline shift from experiment to experiment. This variation in baseline is attributed to slight variations in the temperature calibration of the furnace and possibly ambient climate fluctuations from experiment to experiment. It is noted that the slopes for each experiment are all within close agreement for each experimental run, and the observed baseline offset suggests that there is a different number of conduction electrons or total oxygen vacancies available for the same film and gas exposure conditions. This seems unlikely since the Au-YSZ film did not experience additional doping between experiments, but what is more likely is that there were slight variations in the thermal ramp up in temperature and likewise the cooling period between experiments. It is true that the equilibrium constant K is temperature dependent, where $K=exp(-\Delta G/RT)$ with $-\Delta G$ representing the change in Gibbs free energy and R the molar gas constant, thus a temperature fluctuation should also be reflected in a change of slope for the different experiments, but a five Kelvin deviation in the 773.15 K operating temperature, our estimated error in operation temperature, would only result in a slope shift of $\sim 2 \times 10^{-6}$ rad^2 s^{-2}, which would not be observed in our dataset. As for the temperature dependence of the peak position baseline, it has been observed by this group that the peak position and FWHM of the SPR band for Au-YSZ films is very sensitive to variations in temperature, where a change in five Kelvin can result in a 0.1 nm peak position shift, which is still an order of magnitude lower than what would account for the peak position baseline shift observed in Figure 13, but it does point to the sensitivity of optical absorption of the AuNPs to non electrochemical phenomena for the cause of any baseline shift in peak position. Furthermore, the variation in electrochemical equilibrium would be more likely to cause an overall slope change rather than an overall red or blue shift for all data points as observed in Figure 13. It is still difficult to pinpoint a single factor to blame for this random baseline shift from day to day, but it is proposed that the cause lies on the environmental sensitivity of the AuNP optical properties to non electrochemical interactions, such as surface plasmon phonon scattering.

Since it is of interest to this group to monitor charge transfer due to the Au-YSZ thin films reaching electrochemical equilibrium by transferring electrons from AuNPs to and from diffusing oxygen ions, examining the change in the square of the peak position in angular frequency as a function of the change in normal partial pressure ratio: $pH_2^{1/4}/pO_2^{1/8}$ removes the spread in data observed in Figure 13 and allows for an estimate of the average total charging occurring per AuNP. Figure 14 displays the change in the square of the peak position data and change in calculated average number of conduction electrons, which has been averaged for each identical gas exposure concentration, plotted versus the change in the gas exposure ratio ($pH_2^{1/4}/pO_2^{1/8}$). The base H_2 concentration used in calculating the change was 0.01 vol. % which was selected to reflect the lower level purity of the exposure gases upon delivery to the exposure chamber. A weighted linear fit with a slope of $(2.27\pm0.04) \times 10^{29}$ rad^2 s^{-2} and an R^2 equal to 0.974 to this data has been added to Figure 14 and forced to intersect the origin. The quality of the fit is again an indication that the proposed electrochemical reaction (4) mechanism is the dominant reaction mechanism which is highlighted through detection using the AuNPs as the

optical beacon for the reaction process. It is apparent from this graph that exposure to these gas mixtures causes the AuNP to experience a charging/discharging ΔN_e from ~600 to 4000 electrons during these redox reactions. Given that the free electron density for gold is 5.9×10^{28} electrons/m^3, this represents a 0.4 % change in conduction electrons for these ~30nm AuNPs.

The change in Gibbs free energy can be estimated for reaction (4), however a number of approximations need to be made; 1) Although the H_2O concentration was not controlled, if an approximate concentration of 0.01 vol. % is used for an H_2O (to account for water impurities in the gas manifold), baseline concentration, 2) The number of conduction electrons in an uncharged AuNP is estimated to be $\sim 3.5 \times 10^5$, and 3) The number of oxygen vacancies per AuNP in a completely reduced Au-YSZ film is $\sim 5.7 \times 10^4$, With these approximations the change in Gibbs free energy for the reaction outlined in (4) is ~ -150 kJ/mol at 500 °C, thus favoring the reduction of the Au-YSZ thin film. This is only a rough approximation and could be off by as much as an order of magnitude, but the sign of this approximate value of ΔG agrees for what is expected for the spontaneous formation of gas phase H_2O by H_2 and $\frac{1}{2}O_2$ at 500 °C. For gas phase reactions this leads to a ΔG of approximately -590 kJ/mol. Qualitatively it is expected that the absolute value of the change in Gibbs free energy for the formation of gas phase H_2O by reacting H_2 with oxidized Au-YSZ thin films at 500 °C should be lower than that for the formation of gas phase H_2O by H_2 and $\frac{1}{2}O_2$ at 500 °C as both the removal of oxygen ions from the YSZ matrix and the subsequent donation of electrons back to the AuNPs upon reaction with gas phase H_2 to form H_2O require an energy cost which is not present in the gas phase reaction.

We have also studied the temperature dependence of the H_2 reaction and as shown in Figure 15 for 1% Hydrogen in air exposures there is no change in the SPR band at room temperature. The reaction onset appears at a lower temperature than observed for the CO reactions at ~200°C, which is still consistent with the onset of the O^{2-} formation on YSZ matrices. The H_2 sensing signal change appears to saturate at 400 and 500°C.

Hydrocarbon Detection – Ethanol at 500°C

As evidenced by the ease of detection of H_2 as detailed above, it is apparent that if a hydrocarbon molecule catalytically reacted on the Au-YSZ nanocomposite film forming H atoms, these would also react with the bound oxygen anions causing a blue shift in the SPR band. Furthermore, it is likely that carbon would possibly also react, similar to the CO reaction detailed above, also causing a blue shift. As the hydrocarbon target of choice can lead to a complicated set of reactions we chose ethanol as our first hydrocarbon target molecule as it a common fuel for a variety of combustion events. Ethanol vapors were picked up and mixed into the gas stream through the use of a bubbler pick-up source. Liquid ethanol was placed in a glass vessel and held at room temperature. The partial pressure of ethanol in this vessel and under these conditions is 70 torr, which when picked up by a volumetric flow, 20sccm of air and mixed with a larger volumetric flow, 1980sccm, leads to a concentration of ethanol that is equal to 900 ppm concentration in a total flow of 2000sccm. By varying the volumetric split of flow through the bubbler we are able to deliver ethanol exposures of 150, 1500 and 5000 ppm for these experiments. Figure 16 displays the change in sensing signal vs. time for these ethanol exposures and it is clear that we are able to reversibly detect ethanol under these conditions. There is an initial spike in the sensing signal upon activation of the ethanol gas pulse and while

more studies are needed, at this point we believe this may be an artifact of the hydrocarbon gas source and delivery lines which in between gas pulses has a mild buildup of ethanol in the ~20' long ¼" tubing. Analysis of the change in the SPR band's peak position and FWHM indicate that the characteristic blue shift and narrowing of the SPR band upon reaction with O^{2-}, leading to electron donation back to the gold nanoparticles is the reaction mechanism for the detection of ethanol with these films. Future studies will optimize the hydrocarbon gas delivery lines to prevent this type of problem. We have performed a total of 20hours of ethanol exposure experiments to date and at this point the detection of 150ppm of ethanol as seen in the figures has quite a bit of contrast which should allow for future studies and development of more sensitive Au-YSZ films for the detection of hydrocarbons. However, of particular interest to the studies is that the Au-YSZ films have no obvious problems with carbon buildup due to the catalytic reaction of ethanol which should produce CO_2 and water as the by-products of this reaction. These initial conclusions are from analysis of the SPR band of the Au-YSZ sample prior to any ethanol exposure and then after 12 and then 19 hours of experiments. These three SPR bands are overlaid and displayed in Figure 17. As can be seen we see a change in the SPR band after the initial 12hr experiment but then there is no measurable change in the SPR band after another 7 hrs of experiments with ethanol concentrations of 150, 1500 and 5000 ppm in air at an operating temperature of 500°C. A detailed materials analysis of the Au-YSZ film after much longer exposures, month long studies, is still required to determine the extent of carbon buildup but these initial experiments are promising from a sensitivity and stability standpoint. Furthermore, a detailed particle size dependence study for the detection of hydrocarbons should also be performed for optimization of hydrocarbon detection.

NO_2 Sensing Studies

Oxides of nitrogen (NO_x) are one of the main contributors to the formation of tropospheric ozone, which has been linked to respiratory conditions in humans, such as degradation of lung tissue, and reduction of lung function. NO_x is also a factor in the formation of acid rain and nutrients that degrade water quality.[5] In order to further lower the NO_x emissions from current man made sources, active emission control systems will have to become more sophisticated. In particular what is required to reduce NO_x emissions are NO_x sensors that operate at temperatures between 500-800 °C. Currently, there is no technology available that can reliably sense NO_x at temperatures ranging from 500-800 °C. Sensors based on field effect devices and solid oxide semiconductors are small and cost effective, but experience stability issues above ~600 °C due to degradation of electrical junctions and nonlinear electrical behavior. Optical methods such as fluorescence, can also detect the production of NO_x by jet engines, but fluorescence measurements require a short wavelength, high power laser to excite NO_x molecules to photo emit, as thermal excitation is not possible at typical exhaust gas temperatures. Laser induced fluorescence is an extremely accurate method for detecting low levels of NO_x, unfortunately it is not a practical method for measuring NO_x emissions due to the size and expense of high power lasers and other optical equipment required to capture the fluorescence spectra. The NO_2 studies utilized the oxygen ion conduction properties of metal oxides combined with the catalytic reactivity of gold nanoparticles to develop a novel all-optical method for the detection of emission gases at operating temperatures ranging from 500 to 800 °C.

Theoretical Calculations:

A similar theoretical description of the optical properties of the AuNPs as a function of exposure to NO_2 and O_2 has been developed with a few differences in the chemical reactions and resulting

equations as outlined below. As mentioned previously, exposure to varying concentrations of NO_2 and O_2 in N_2 at 500 °C has been performed which both reduces and oxidizes the YSZ matrix so it is crucial to build an understanding for how charge is expected to transfer to and from the AuNP upon various exposure conditions. For this a half reaction can be written in Kröger-Vink notation for the oxidation of the YSZ matrix by gas phase NO_2:

$$\mathrm{NO}_{(g)} + \mathrm{O}_{\mathrm{O}}^{\times} + 2\mathrm{Y}'_{\mathrm{Zr}} \longleftrightarrow \mathrm{NO}_{2(g)} + \mathrm{V}_{\mathrm{O}}^{\bullet\bullet} + 2\mathrm{Y}'_{\mathrm{Zr}} + 2\mathrm{e}'_{\mathrm{AuNP}}, \tag{10}$$

and another half reaction can be written for the oxidation of the YSZ matrix by gas phase O_2:

$$\mathrm{O}_{\mathrm{O}}^{\times} + 2\mathrm{Y}'_{\mathrm{Zr}} \longleftrightarrow \frac{1}{2}\mathrm{O}_{2(g)} + \mathrm{V}_{\mathrm{O}}^{\bullet\bullet} + 2\mathrm{Y}'_{\mathrm{Zr}} + 2\mathrm{e}'_{\mathrm{AuNP}}. \tag{11}$$

By combining the two previous half reactions we can derive a reaction equation that accounts for the charge transfer reactions at varying concentrations of NO_2 and O_2:

$$\mathrm{NO}_{(g)} + 2\mathrm{O}_{\mathrm{O}}^{\times} + 4\mathrm{Y}'_{\mathrm{Zr}} \longleftrightarrow \mathrm{NO}_{2(g)} + \frac{1}{2}\mathrm{O}_{2(g)} + 2\mathrm{V}_{\mathrm{O}}^{\bullet\bullet} + 4\mathrm{Y}'_{\mathrm{Zr}} + 4\mathrm{e}'_{\mathrm{AuNP}}. \tag{12}$$

When at equilibrium the full reaction can be written in terms of the equilibrium constant *K*:

$$K = \frac{p\mathrm{NO}_2 p\mathrm{O}_2^{1/2} N_{\mathrm{V}_\mathrm{O}^{\bullet\bullet}}^2 N_{\mathrm{e}}^4}{p\mathrm{NO} N_{\mathrm{O}_\mathrm{O}^{\times}}^2}, \tag{13}$$

where $p\mathrm{NO}$, $p\mathrm{NO}_2$, and $p\mathrm{O}_2$ represent the numeric value of the partial pressures of NO, NO_2 and O_2, respectively, and $N_{\mathrm{O}_\mathrm{O}^{\times}}$, $N_{\mathrm{V}_\mathrm{O}^{\bullet\bullet}}$ and N_{e} correspond to the number of filled oxygen vacancies, unfilled oxygen vacancies and AuNP conduction electrons per film volume containing one AuNP and the corresponding YSZ per AuNP. For this model we assume that the total positive charge of the AuNP is equal to two times the number of filled oxygen vacancies ($N_{\mathrm{O}_\mathrm{O}^{\times}}$) and that the number of unfilled vacancies ($N_{\mathrm{V}_\mathrm{O}^{\bullet\bullet}}$) is equal to the total number of vacancies available when the AuNP is uncharged ($N_{\mathrm{V}_\mathrm{O}^{\bullet\bullet}0}$) minus the total number of filled oxygen vacancies ($N_{\mathrm{O}_\mathrm{O}^{\times}}$). With these assumptions, (13) can be reformulated as the following:

$$\frac{K^{1/2} p\mathrm{NO}^{1/2}}{p\mathrm{NO}_2{}^{1/2} p\mathrm{O}_2^{1/4} N_{\mathrm{e}}^2} = \frac{2N_{\mathrm{V}_\mathrm{O}^{\bullet\bullet}0}}{N_{\mathrm{e}0} - N_{\mathrm{e}}} - 1, \tag{14}$$

where $N_{\mathrm{e}0}$ denotes the number of conduction electrons in an uncharged AuNP. Simplifications can be made to (14) if it is assumed that the number of unfilled oxygen vacancies is always greater than the number of filled oxygen vacancies which results in the following quadratic equation:

$$\frac{2N_{\mathrm{V}_\mathrm{O}^{\bullet\bullet}0} p\mathrm{NO}_2{}^{1/2} p\mathrm{O}_2^{1/4}}{K^{1/2} p\mathrm{NO}^{1/2}} N_{\mathrm{e}}^2 + N_{\mathrm{e}} - N_{\mathrm{e}0} \cong 0. \tag{15}$$

By solving the quadratic equation and making simplifications based on the magnitude of $N_{\mathrm{V}_\mathrm{O}^{\bullet\bullet}0}$ and $N_{\mathrm{e}0}$, the relation that correlates the number of conduction electrons per AuNP to the exposure gas partial pressures, $N_{\mathrm{V}_\mathrm{O}^{\bullet\bullet}0}$, $N_{\mathrm{e}0}$, and the equilibrium constant is the following:

$$N_{\mathrm{e}} \cong \sqrt{2}\left(\frac{K^{1/2} N_{\mathrm{e}0} p\mathrm{NO}^{1/2}}{N_{\mathrm{V}_\mathrm{O}^{\bullet\bullet}0}}\right)^{1/2} \frac{1}{p\mathrm{O}_2^{1/8} p\mathrm{NO}_2^{1/4}}. \tag{16}$$

By solving (1) for N_e and combining it with (16) one is left with an equation where the square of the SPR band peak position should vary linearly with $p\mathrm{O}_2^{-1/8} p\mathrm{NO}_2^{-1/4}$:

$$(\omega_1)^2 = \sqrt{2}\left(\frac{3e^2}{(1+2\varepsilon_m) m_e 4\pi\varepsilon_0 R^3}\right)\left(\frac{K^{1/2} N_{\mathrm{e}0} p\mathrm{NO}^{1/2}}{N_{\mathrm{V}_\mathrm{O}^{\bullet\bullet}0}}\right)^{1/2} \frac{1}{p\mathrm{O}_2^{1/8} p\mathrm{NO}_2^{1/4}} \tag{17}$$

Results and Discussion:

The primary explanation for shifts in the peak position of the SPR band is charge exchange from the AuNPs in the YSZ matrix to diffusing oxygen ions from catalytic reactions occurring within the Au-YSZ nanocomposites, as outlined in the previous section. Evidence for this theory can be seen in Figure 18 where, in the presence of a matrix oxidizing, 20 vol. % O_2, baseline gas exposure (air), exposure to NO_2 results in a red-shift of the SPR band peak position due to the removal of charge from the AuNP by the O atom produced upon dissociation of NO_2 on the AuNP. It is interesting to note that while the optical response of the AuNP towards O_2 in N_2 is saturated at levels above 10 vol.%, the addition of the oxidizing species, NO_2, causes a further red shift in the SPR band at concentrations ranging from 5 to 100ppm in an air carrier gas. A similar 5 ppm increase in O_2 concentration, in the air carrier gas, would not be measurable due to the matrix being saturated with the oxygen baseline reactions.[6] While it is not fully understood why an O_2 saturated Au-YSZ nanocomposite is susceptible to the addition of NO_2, it is likely due to a difference in the interfacial reaction sites available to the two species which may also include the specific oxygen vacancy type, Y-Y, Y-Zr and Zr-Zr that is available for stabilization of the generated oxygen ion species.

The FWHM of the SPR band of the Au-YSZ nanocomposite also responds to the exposure of NO_2. Upon oxidation the FHWM of the SPR band is expected to broaden, as observed previously, and it is this characteristic broadening upon oxidation of the Au-YSZ film by NO_2 that is displayed in Figure 19b. As mentioned in the previous section, the peak position of the SPR band is a convenient parameter to monitor charge transfer from AuNPs to diffusing oxygen ions, but the FWHM can be indicative of other physical phenomena. The FWHM of the SPR band is related to the relaxation time of the oscillating quasi-free electron cloud and this relaxation time can be affected by several nanoparticle and matrix parameters, such as particle size, matrix defects, phonon scattering, charge density and adsorbates. As the last two parameters listed are being varied upon exposure it is these two that need to be considered as being responsible for the broadening of the SPR band. Simple free-electron theory states that the FWHM is inversely proportional to the free electron density. This means that as the Au-YSZ nanocomposite is oxidized and electrons are removed from the AuNPs the SPR band should broaden, which is observed. Nevertheless, electron density affects should have a minimal affect on SPR band broadening since a 28 nm AuNP would have upwards of 6×10^5 conduction electrons and, as approximated by the peak position change in the SPR band, the greatest number of electrons removed by exposure to 100 ppm NO_2 is roughly 7×10^2 electrons, therefore only 0.1 % of the free electrons are available for affecting the FWHM. This would only result in a ~0.2 nm broadening in the SPR band upon exposure to 100 ppm of NO_2 if the change in free electron density was the only phenomenon causing the dampening of the SPR band.

Another source of SPR band broadening are the diffusing oxygen ions. Adsorbate induced dampening was first experimentally shown on metal nanoparticles in cryogenic conditions but it is possible that a similar phenomenon is being observed upon oxidation of the Au-YSZ nanocomposite. Upon exposure to a matrix oxidizing gas such as NO_2, an oxygen ion can diffuse into the YSZ matrix after catalytically dissociating from NO_2 forming gas phase NO. It is assumed that after dissociation the oxygen ion would likely diffuse to the closest unfilled oxygen vacancy near a AuNP, given that the temperature is above the oxygen ion diffusion barrier for the matrix. While electrostatically drawn to the oxygen ion vacancy closest to the now charged AuNP, the oxygen ion has now changed the matrix environment closest to the

AuNP and can act as a trap state for the optically driven oscillating quasi-free electrons of the AuNP. More work must be performed to better understand the defect energies of these diffusing oxygen ions with respect to the Fermi energy of the nanocomposite, but early calculations based on defect energies obtained for bulk YSZ show promise for adsorbate induced dampening playing a role in the broadening of the SPR band.

After examining the raw exposure data, calibration curves for the change in peak position and FWHM are determined for the various concentrations of NO_2 in an air carrier gas, which are displayed as the insets in Figure 19A and 19B. Figure 20 displays the change in peak position for NO_2 in varying concentrations of O_2. As one would expect, Figure 20 shows that the response to NO_2 increases as the O_2 concentration is decreased. Figure 20 only shows the change in peak position as a function of NO_2 concentration as it is this parameter that relates to charge transfer between the AuNP and diffusing oxygen ions and can most easily be related to the electrochemical equilibrium equation (12) and the SPR peak position equation (17).

By plotting the square of the change in peak position in angular frequency squared as a function of the change in the gas partial pressure product: $pO_2^{-1/8} pNO_2^{-1/4}$ linear characteristics are observed as displayed in Figure 21. The change in square of the peak position is plotted as a function of the change in $pO_2^{-1/8} pNO_2^{-1/4}$ because a random baseline shift is observed as a function of temperature ramp cycles, repositioning the SPR band peak position from experiment to experiment by fractions of a nanometer. This shift is slight, but it is enough to make a difference when the maximum shift observed upon exposure to 100 ppm NO_2 is only ~0.7 nm. To calculate the change in $pO_2^{-1/8} pNO_2^{-1/4}$, the initial concentration of NO_2 is set at 3.2 ppm for each of the different oxygen concentrations as this concentration is just below the lower detection limit of NO_x for the Au-YSZ nanocomposite. A linear relation is expected from (17) if it is assumed that the particle size, equilibrium constant, partial pressure of NO, and dielectric function of the matrix remain unchanged for all exposure conditions. The theoretical change in number of electrons per AuNP calculated from (17) has been added to the secondary ordinate which reiterates the earlier statement that the maximum number of electron removed per nanoparticle upon exposure to 100 ppm NO_2 is predicted to be $\sim 7 \times 10^2$. With an R-squared equal to 0.975 the linear fit, which was forced though the origin, agrees quite well with the plotted data. As the equilibrium equation and subsequent relation of peak position to gas partial pressures for NO_2 in O_2 is different than that for H_2 and O_2 exposure, $pH_2^{1/4} / pO_2^{1/8}$, observed previously by this group, the data set acts as a further clarification for the proposed electrochemical reaction mechanism for both oxidizing and reducing gases reacting within the Au-YSZ nanocomposite film.

Lastly, it is important to address the temperature dependence of the optical response of Au-YSZ films to variations in gas exposure concentration. Plotted in Figure 22 is the SPR band signal versus time for a Au-YSZ nanocomposite film exposed to ~1 hour cycles of air and 5, 10, 50, and 100 ppm NO_2 in air at 200, 300, 400, 500, 600, and 700 °C. The signal is a measure of the minimum to maximum difference of the SPR band subtracted from the first spectrum taken within a given set of gas exposures. An offset has been added the exposure curves at higher temperatures to make the Figure easier to read. Upon exposure to NO_2 an increase in signal is observed and upon NO_2 removal the signal returns to the baseline value. Not only is the magnitude of the signal change of interest but the response time required to achieve this signal change is indicative of the reaction kinetics and the diffusion times of the species. As expected,

the signal change becomes observable for the data set with an operating temperature of 300 °C which is approximately the thermal activation energy for oxygen ion diffusion for YSZ. Once oxygen ion conductivity is thermally activated, a sharp increase in the signal change towards NO_2 is observed by raising the exposure temperature to 400 °C. By increasing the temperature beyond 400 °C the signal change decreases as the temperature is increased and the response and recovery times decrease to their minimum values at 500 °C. The decrease in the response and recovery time can be attributed to increased mass transport kinetics at higher temperatures and the minimum reached is limited by the rate of gas surface sampling on the Au-YSZ nanocomposite achievable by the flow cell setup. What is particularly interesting is the decrease in signal change as the temperature is increased above 400 °C. The thermal dependence of the signal change is what will define the operational temperature limits. Using a high temperature Kelvin probe, M. Yamawaki et al. have observed that a 10 mol % yttria doped bulk YSZ sample without an electronic conductor attached to the reaction site, is oxidized in the presence of O_2 at temperatures ranging from 500 to 900 °C.[7] Also observed by M. Yamawaki et al. was an ~60 % increase in O^- surface coverage upon an increase in temperature from 500 to 700 °C after which a decrease in O^- surface coverage was observed as the temperature was increased above 700 °C. Additional evidence of this reduction in response to NO_2 has also been observed for potentiometric electrochemical sensors which use YSZ as a solid electrolyte where the greatest potential is observed at 700 °C.[8] Nowotny et al. have also observed a decrease in O^- surface coverage on YSZ at temperatures above 700 °C, with an approximate maximum at ~725 °C.[9]

It has been proposed that the charge transfer mechanism for O_2 first relies on adsorption of O_2 onto the YSZ surface and donation of an electron by the matrix to form an O_2^- species. After which, a dissociation of O_2^- into two O^- species on the surface of the YSZ matrix is expected after the donation of another electron by the matrix. Finally another electron can be donated to the O^- species forming O^{2-}, which can then be taken up by the vacancies in the YSZ matrix.[9] We propose that an increase in the O^- species surface coverage at elevated surface temperatures may be causing the reduction in the NO_2 sensing signal for the same reason one would expect it to reduce the uptake of oxygen by YSZ. As demonstrated by the change in the SPR peak position and FWHM observed upon exposure to NO_2, it is proposed that exposure to NO_2 results in an uptake of O^{2-} by the YSZ matrix and if NO_2 must first dissociate at the Au-YSZ surface into gas phase NO and chemisorbed O^- then a reduction in surface area available for NO_2 to react, should result in a reduction in the measured signal change. Indeed the data in Fig 5 shows an ~60% reduction in signal change towards 100 ppm NO_2 in air with an increase in operation temperature from 500 to 700 °C, consistent with the reduction observed by Yamawaki for bulk YSZ samples.

Conclusions

We have performed a series of experiments to determine the proof of concept for using Au-YSZ nanocomposite films for the detection of CO, NO_2, H_2 and ethanol under harsh environment conditions. These experiments have shown that for CO, H_2 and ethanol that there is a reaction with the O^{2-} ions which occupy vacancies in the YSZ matrix that form an oxidized product with the electrons from the oxygen anion being donated back to the Au nanoparticles that induces the characteristic blue shift of the SPR band. The temperature and oxygen titration experiments confirm that for this reaction to take place, the operation temperature must be above the threshold required for formation of O^{2-} from the background oxygen and if there is no background oxygen or the temperature is below this formation threshold the reaction is

deactivated and sensing is not possible. For the studies performed here the operation temperature needs to be above 400 °C with 500 °C being preferable. Likewise the oxygen titration experiments determined that for CO and H_2 as long as the oxygen levels are above ~8% the reactions are independent of the oxygen concentration. Experiments to determine the oxygen and temperature dependences of the hydrocarbon reactions will need to be done in a future phase of this program. The NO_2 reaction proceeds through the catalytic reduction of NO_2 on hot gold surfaces to form NO and an O atom. The oxygen atom then forms an O^{2-} ion thus removing electrons from the gold nanoparticle causing the characteristic redshift of the SPR band. For this reaction background oxygen actually reduces the signal contrast and by reducing these levels to 5 and 10vol.% the sensing signal for NO_2 increases as there are more sites available for the formation of a O^{2-} ion as the sample is not saturated from the background oxygen concentration. Therefore the detection of NO_2 is dependent on the background oxygen levels even between 5 and 20vol.% oxygen and is also dependent on temperature as it does have to be above the threshold for O^{2-} formation.

The detection limits for NO_2 were determined to be 5ppm in an air carrier gas and at 500°C. The detection limits for CO were not pushed strongly but at 1000ppm still showed strong signal changes implying that 100ppm detection limits with these initial films is likely possible. For the H_2 studies we were able to detect concentrations as low as 500ppm with strong signal to noise ratios implying a detection limit of ~250ppm. Since the ethanol studies have only been preliminary detection limits cannot be estimated however the significant result from these studies is that they did not appear to become poisoned with carbon within the 20hrs of run time thus performed. Furthermore, all of the films used for this study have shown to be quite rugged and within the lifetime of this study have not shown any significant degradation with time or chemical exposure. Therefore in conclusion it appears that the all-optical detection of CO, H_2, NO_2 and hydrocarbons using the optical signature of Au nanoparticles embedded in a YSZ matrix has shown strong promise for use as a harsh environment compatible chemical sensor.

Acronyms

SPR	Surface plasmon resonance
CCD	charge coupled device
XRD	x-ray diffraction
RBS	Rutherford backscattering spectroscopy
SEM	scanning electron microscopy
Uv-vis	ultra-violet to visible
YSZ	yttria stabilized zirconia
SOFC	solid oxide fuel cell
IC	innovative concepts
rf	radio frequency

Figures

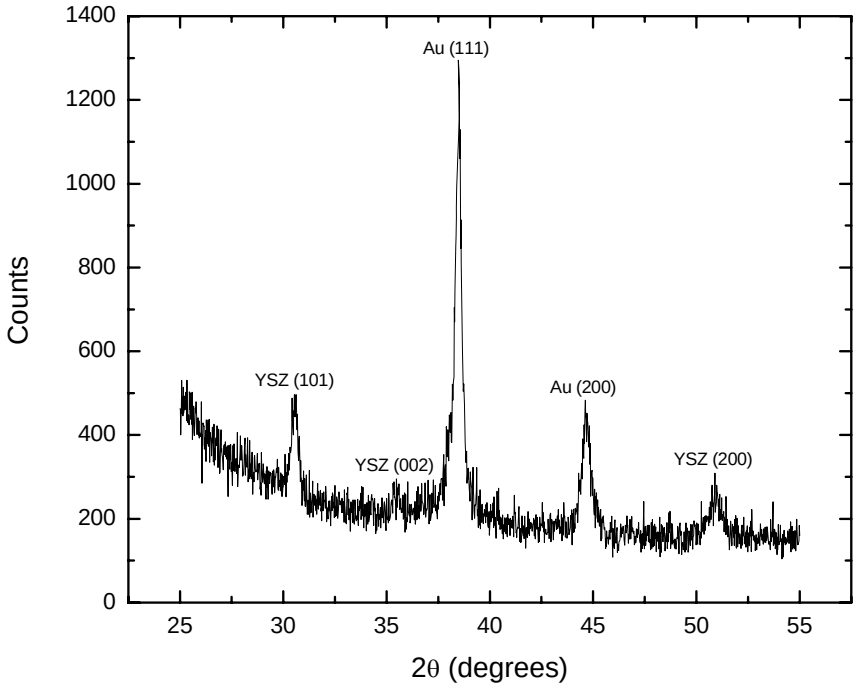

Figure 1. Theta - 2 theta XRD scan data for a typical Au-YSZ thin film.

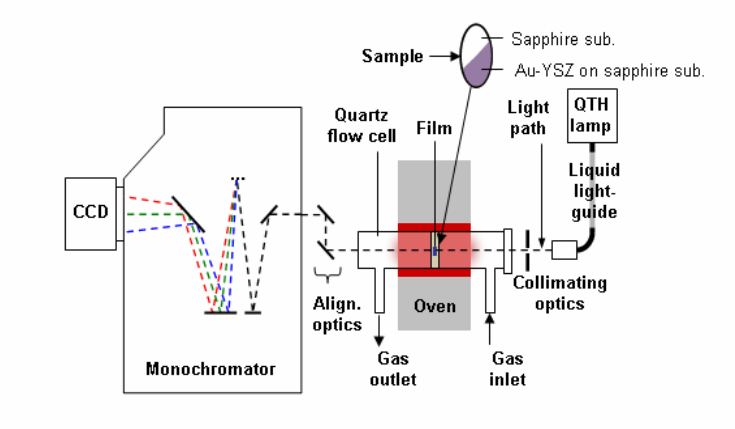

Figure 2: Schematic of the high temperature gas exposure bench utilized for the acquisition of optical absorption data.

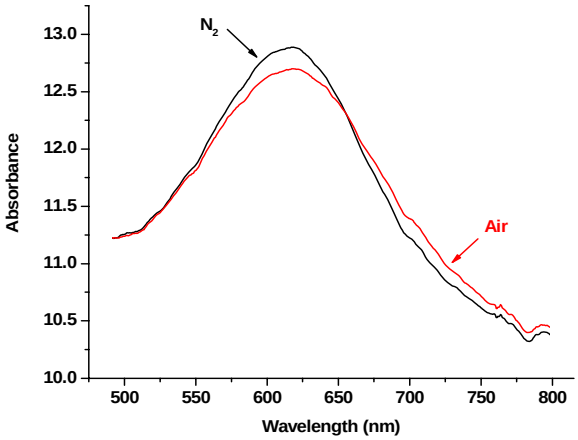

Figure 3: Au nanoparticle SPR band in an air or a N_2 carrier gas at 500°C

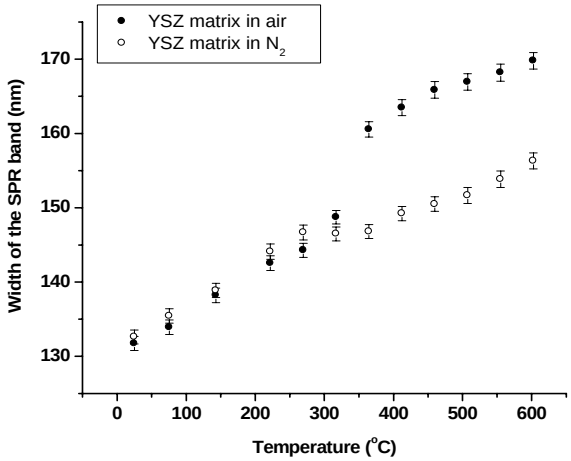

Figure 4: FWHM of the Au SPR band as a function of operating temperature for both air and N_2 carrier gases

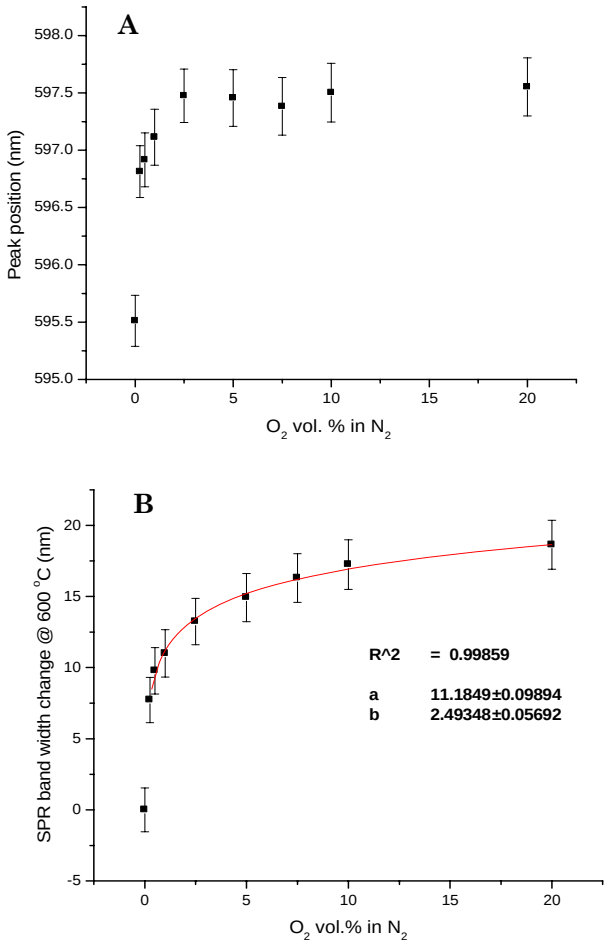

Figure 5: A) Peak position of the Au SPR band vs. O_2 concentration, B) FWHM of the Au SPR band vs. O_2 concentration

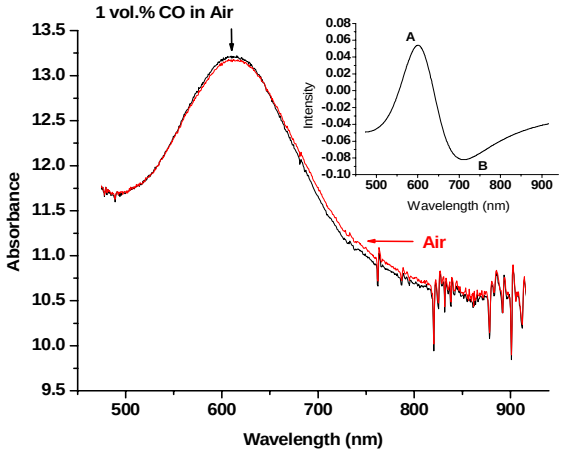

Figure 6: Absorption spectra for air and 1 vol. % CO in air exposures at 500 °C. The insetted graph displays the difference spectrum obtained by subtracting the fitted data resulting from the air and the air/CO exposures

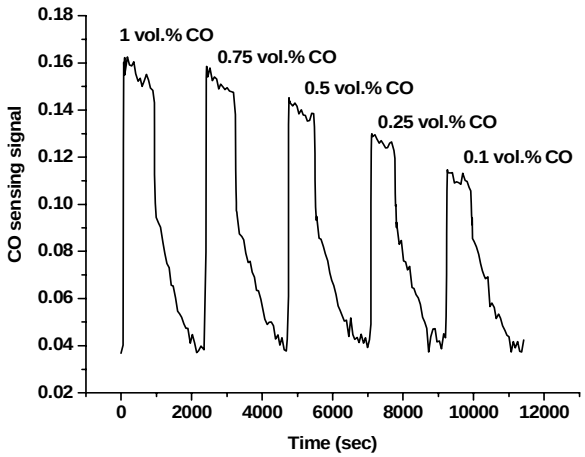

Figure 7: CO sensing signal vs. time for sequential cycles of CO/air and air gas pulse exposures

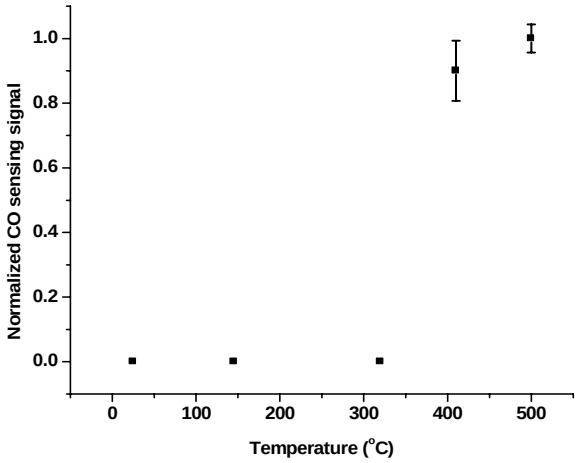

Figure 8: CO sensing signal for 1% exposures as a function of the reaction temperature

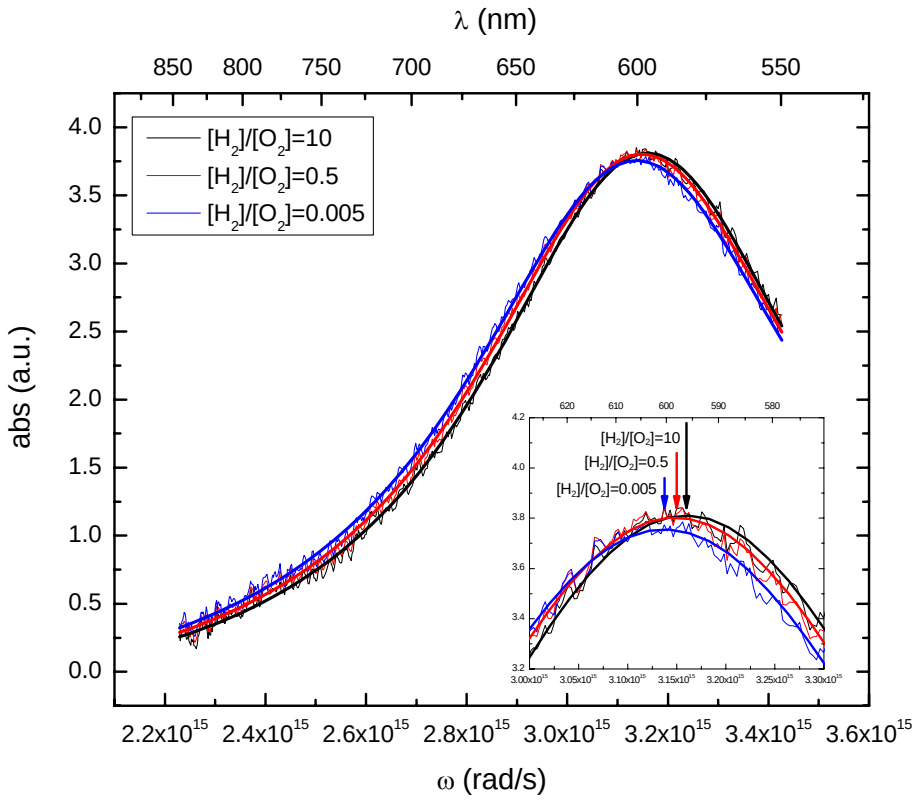

Figure 9: Typical SPR band data and Lorentzian fits for a Au-YSZ film under various redox conditions at 500 °C.

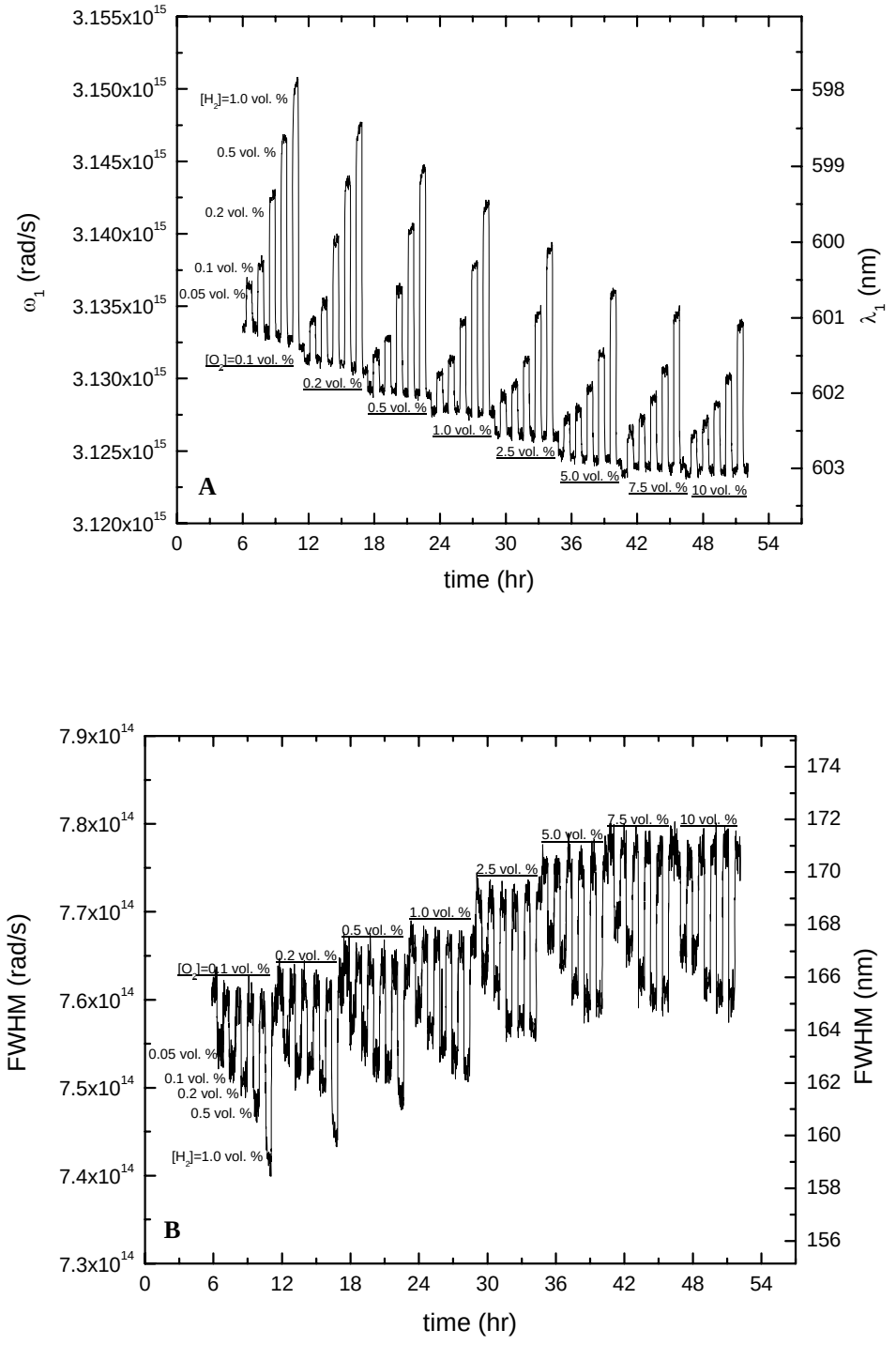

Figure 10 High temperature exposure data of (A) the peak position and (B) the FWHM for a Au-YSZ film at 500 °C under exposure to varying amounts of H_2 and O_2 in N_2.

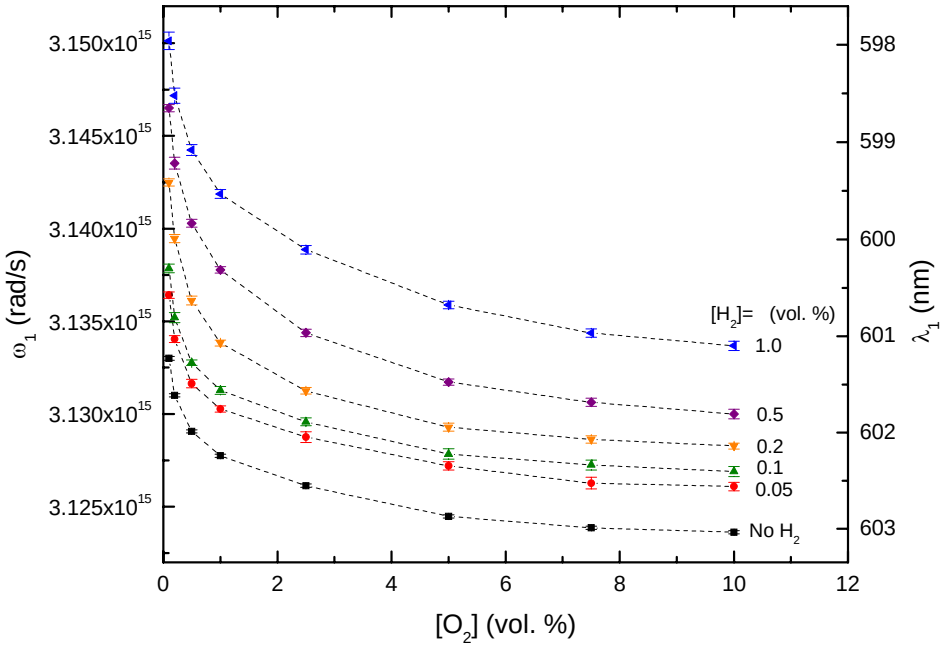

Figure 11 SPR band peak position as a function of O_2 concentration at various concentrations of H_2 for one experimental run.

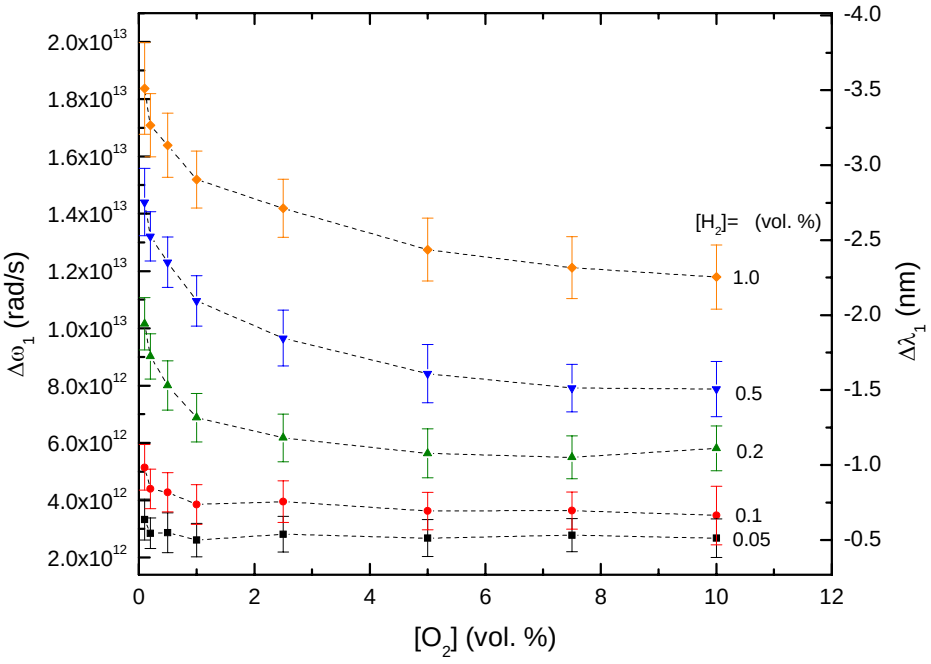

Figure 12 Change in SPR band peak position as a function of O_2 concentration upon exposure to various concentrations of H_2 averaged over four experimental runs.

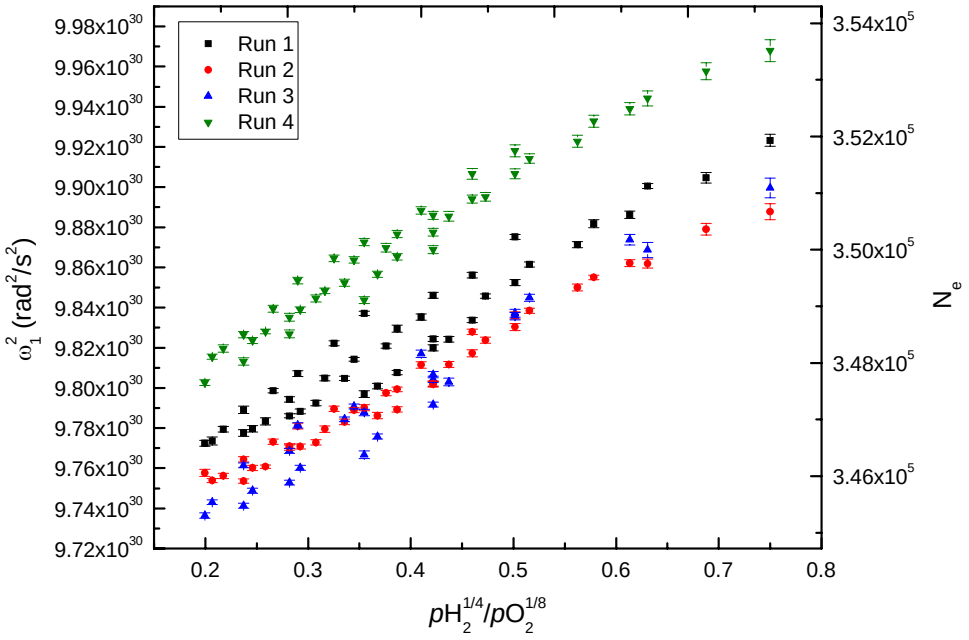

Figure 13 The square of the SPR band peak position and calculated number of conduction electrons per nanoparticle as a function of $pH_2^{1/4}/pO_2^{1/8}$ for all four experimental runs.

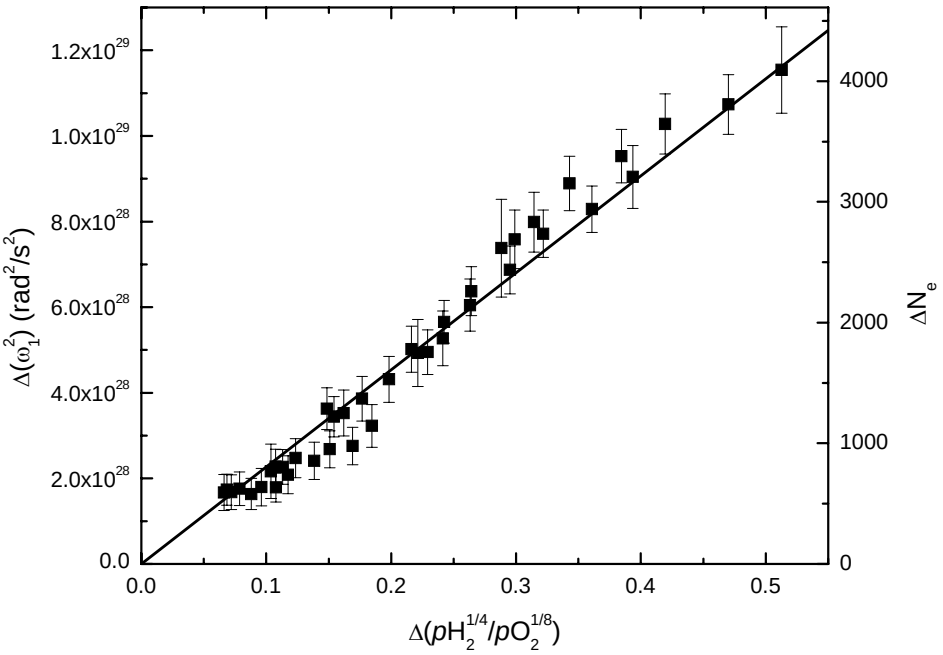

Figure 14 The change in the square of the SPR band peak position and change in calculated number of conduction electrons per nanoparticle as a function of the change in gas mixture ratio: $pH_2^{1/4} / pO_2^{1/8}$ averaged over four experimental runs.

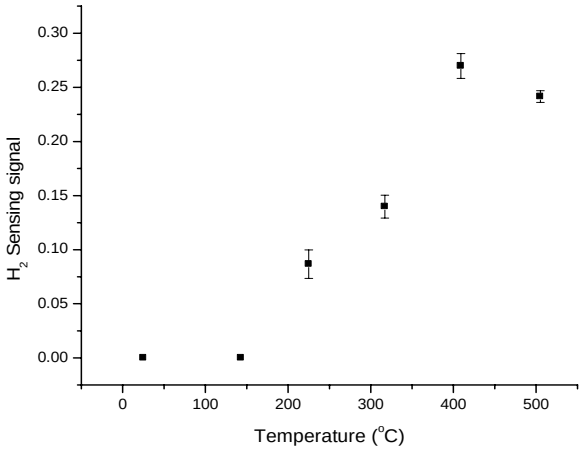

Figure 15: Sensing signal dependence on temperature for 1% H_2 in air exposures

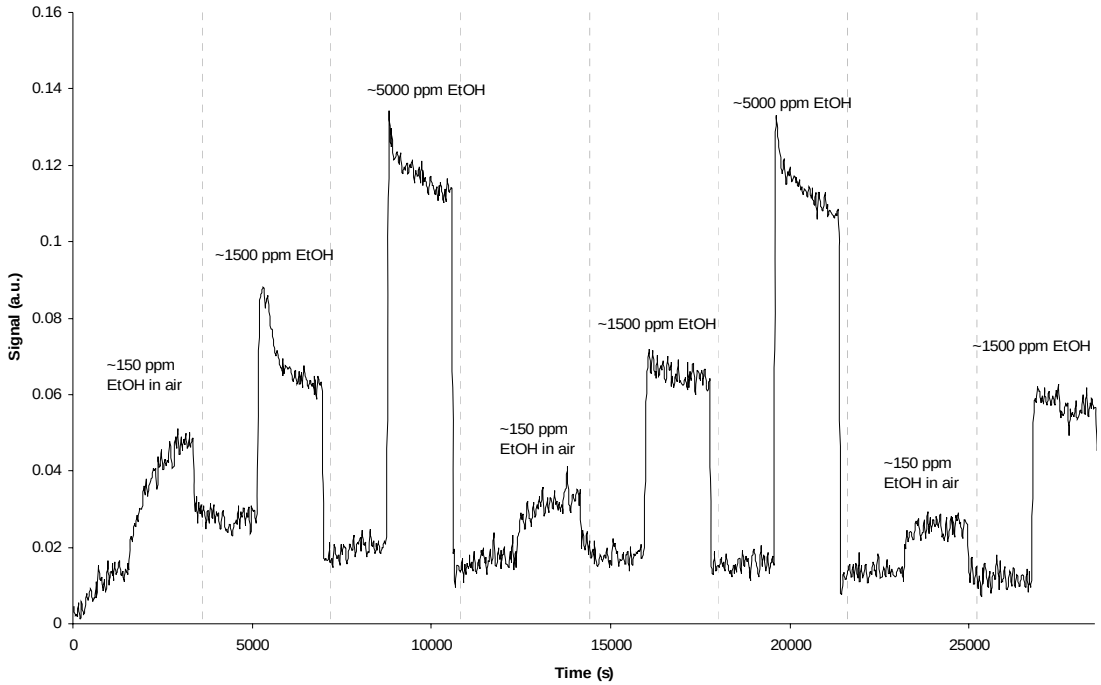

Figure 16: Ethanol sensing signal vs. time for ethanol exposures on the 10nm diameter Au nanoparticle film

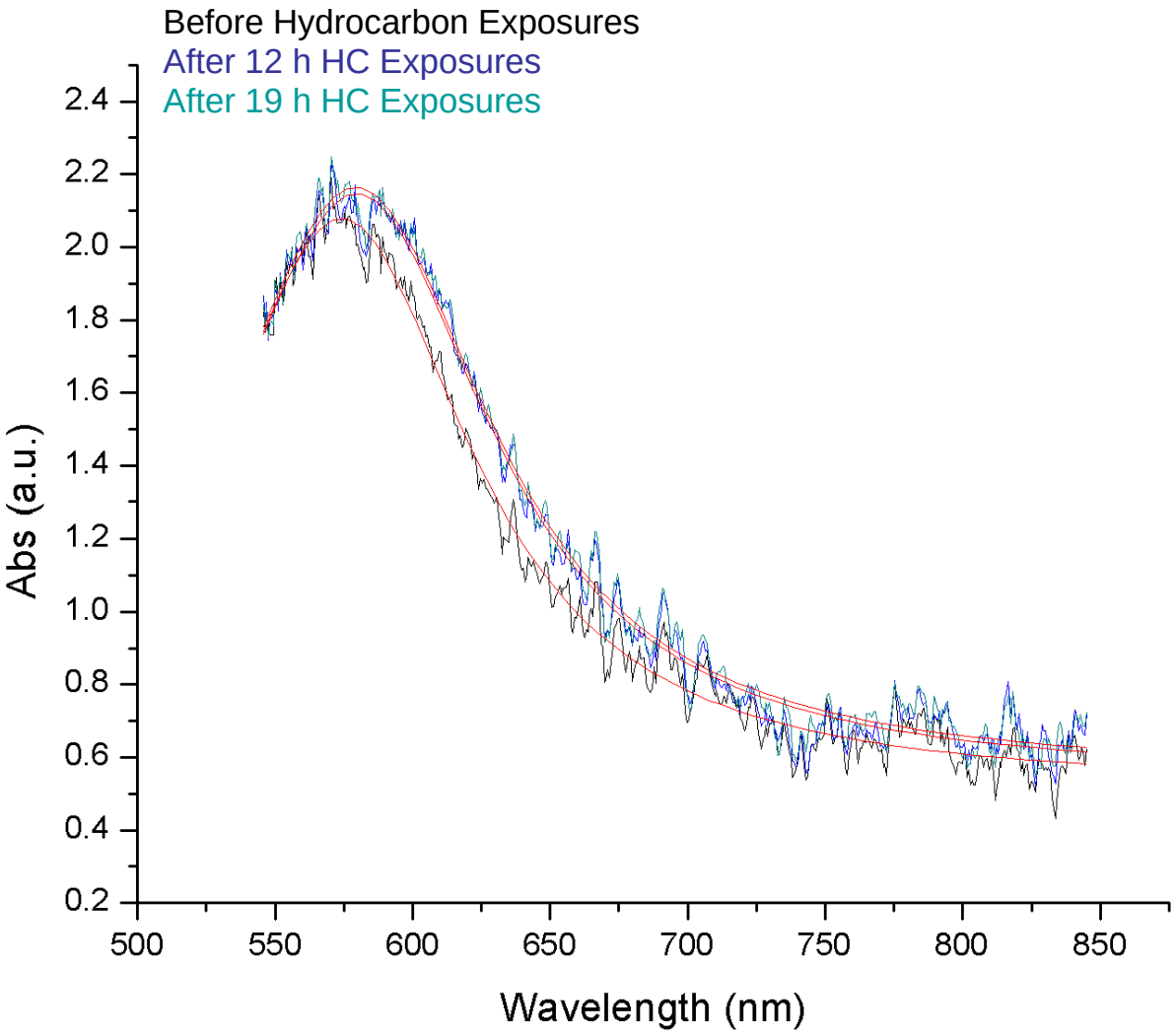

Figure 17: SPR bands for the 10nm diameter Au nanoparticle film before ethanol exposure and after 12 and 19hrs of ethanol sensing experiments

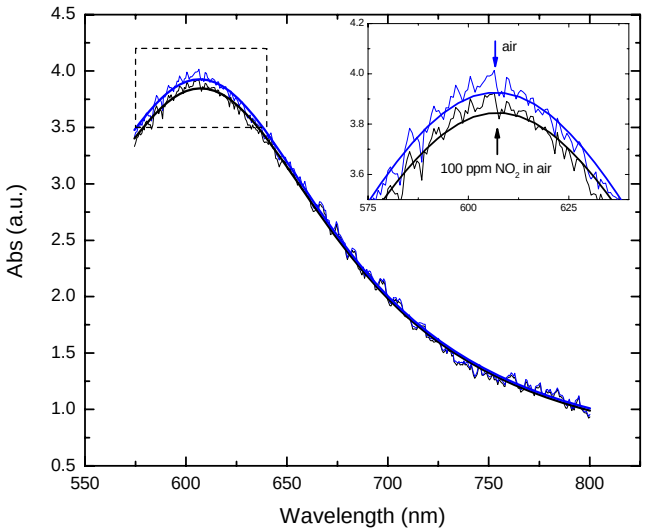

Figure 18: Typical SPR band data and Lorentzian fits for a Au-YSZ film exposed to air and 100 ppm NO_2 in air at 500 °C.

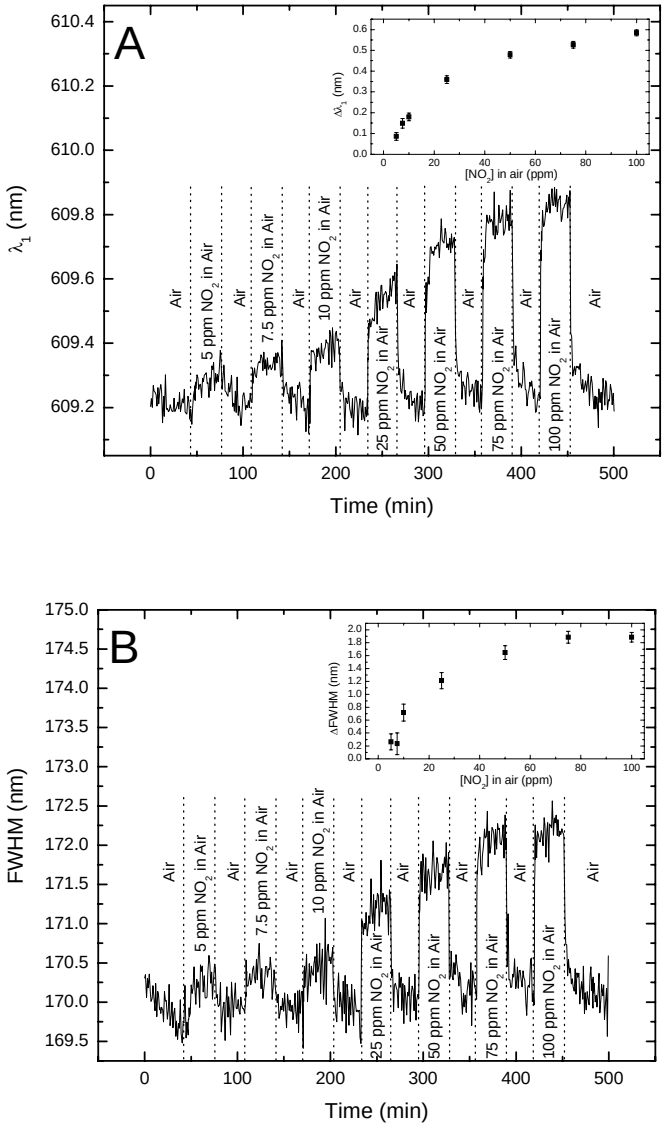

Figure 19: High temperature exposure data of (A) the peak position (λ_1) and (B) the FWHM for a Au-YSZ film at 500 °C under exposure to varying amounts of NO_2 in air. The inset of each plot displays the calibration curve composed for three separate exposure cycles to concentrations of NO_2 from 5 ppm to 100 ppm in air.

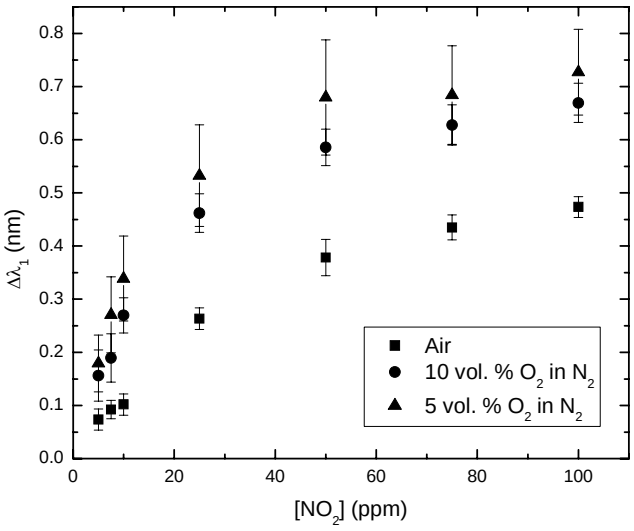

Figure 20: Change in SPR band peak position as a function of NO_2 concentration at various concentrations of O_2 in N_2 averaged over three exposure cycles acquired at 500 °C.

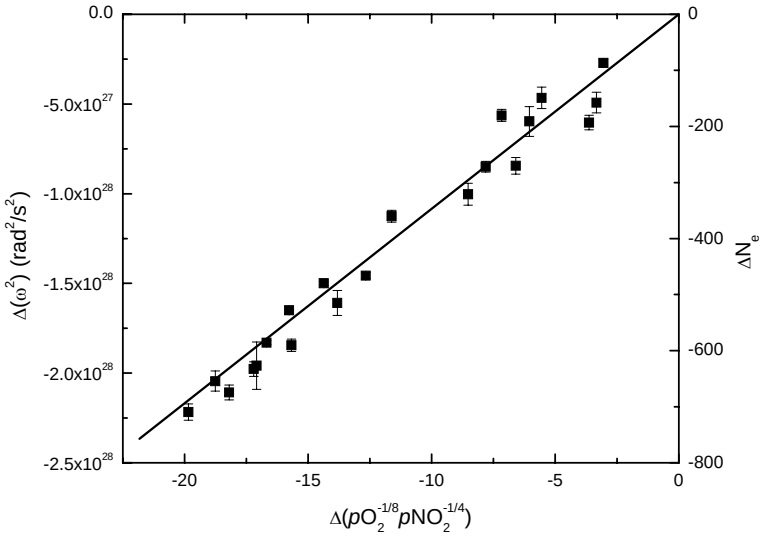

Figure 21: The change in the square of the SPR band peak position and change in calculated number of conduction electrons per nanoparticle as a function of the change in gas mixture product: $pO_2^{-1/8}\,pNO_2^{-1/4}$ averaged over three exposure cycles acquired at 500 °C.

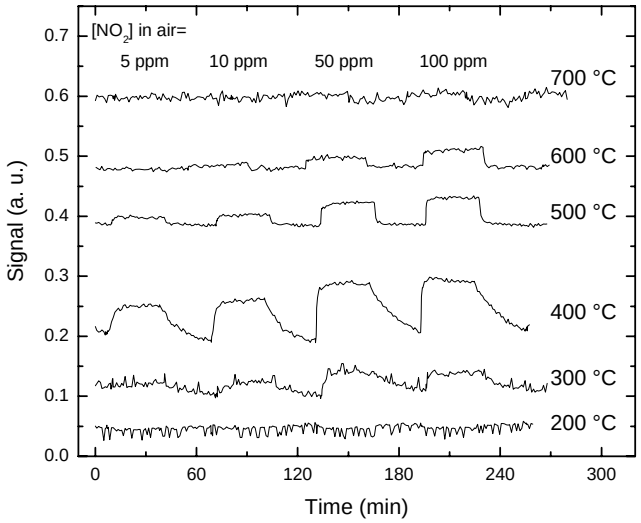

Figure 22: SPR band signal as a function of time for a Au-YSZ film exposed to air (signal decrease) and 5, 10, 50 and 100 ppm NO_2 in air (signal increase) at 200, 300, 400, 500, 600 and 700 °C.

References

[1] G. Sirinakis, R. Siddique, I. Manning, P. H. Rogers, M. A. Carpenter "Development and Characterization of Au-YSZ Surface Plasmon Resonance Based Sensing Materials: High Temperature Detection of CO", J. Phys. Chem. B, **110**, 13508 (2006).

[2] Sirinakis, G.; Siddique, R.; Dunn, K. A.; Efstathiadis, H.; Carpenter, M. A.; Kaloyeros A. E.; Sun, L. J. Mater. Res. **2005,** 20, 3320.

[3] Pinchuk, A.; Kreibig, U.; Hilger, A. Surf. Sci. **2004**, 557, 269.

[4] Persson, B. N. J. *Surf. Sci*. **1993**, 281, 153.

[5] Environmental Protection Agency, "Heal and Environmental Impacts of NOx", http://www.epa.gov/air/urbanair/nox/hlth.html, Accessed 10/22/2007.

[6] P. H. Rogers, G. Sirinakis, M. A. Carpenter, "Direct Observations of Electrochemical Reactions within Au-YSZ Thin Films via Absorption Shifts in the Au Nanoparticle Surface Plasmon Resonance", Submitted to J. Phys. Chem. C (2007).

[7] Yamawaki, M., Bak, T., Nowotny, J., Sorrell, C. C., J. Phys. Chem. Solids, 66 (2005) 322-328

[8] Fergus, J. W., Sens. Actuators B, 121 (2007) 652-663

[9] Nowotny, J., Bak, T., Nowotny, M. K., Sorrell, C. C., Adv. Appl. Ceram, 104 (2005) 154-164